Appl. Phys. B 48, 495–505 (1989)

Applied Physics B Photophysics and Laser Chemistry

Cavity Phase-Shift Error Evaluation in a Magnesium Atomic Beam Frequency Standard

E. Bava, A. Godone, and C. Novero

Istituto Elettrotecnico Nazionale G. Ferraris, Strada delle Cacce, 91, I-10135 Turin, Italy

Received 9 September 1988/Accepted 29 November 1988

Abstract. In high resolution atomic or molecular beam spectroscopy, where the Ramsey interrogation method is used, one of uncertainty sources in determining the resonance frequency accurately is the phase-shift of the electromagnetic radiation in the cavity. This phenomenon, which depends on losses and asymmetries, is analyzed in a general way for a transverse atomic beam dimension much larger than the transition wavelength, a case which occurs in Mg or Ca beam frequency standards and the effects of different misalignments in collimated or divergent beams are examined. Numerical evaluations have been performed in the special case of an experimental Mg beam frequency standard. Divergence plays an important role in determining the cavity phase shift frequency error which is reduced about 100 times with respect to the case of a collimated beam.

PACS: 32.80

Although bias and uncertainties in different atomic beam frequency standards are related to physical phenomena all having the same origin, in some cases, a specific analysis is required. In particular, as far as standard based on Mg or Ca submillimeter metastable beams are concerned, care must be taken in evaluating some errors, that the transverse beam dimensions are much larger than the transition wavelengths. In practice, the Mg and Ca transitions suitable for submillimeter frequency standards occur at wavelengths shorter than half a millimeter, whereas the cross-section dimension of the atomic beam can be of the order of 1 cm. Moreover, in such a geometry, inclination and divergence may play a significant role in producing special effects.

The present realization of the Mg beam standard, whose operation frequency is $\nu_0 = 601277157860 \pm 20$ Hz and stability estimate is

$$\sigma_y(\tau) = 8 \times 10^{-12} \tau^{-1/2}, \quad \text{for} \quad 1\,\text{s} \leqq \tau \leqq 100\,\text{s},$$

is described in [1] with some considerations on the main uncertainty sources.

In this paper, attention is focussed on the cavity phase shift bias, since this effect was not specifically analyzed before. As is well known, precise determination of resonance frequency with the two-zone Ramsey interaction technique [2], used in atomic frequency standards, rests on the assumption that the interaction fields are perfectly in phase; therefore as a practical solution, the two zones are part of the same electromagnetic resonator. In practice losses and asymmetries may destroy this ideal assumption and a phase difference φ between the two interaction regions may arise.

An error is then produced because the peak value of the transition probability does not occur when the radiation field angular frequency ω is coincident with the Bohr frequency ω_0, but the maximum corresponds to a frequency $\omega = \omega_0 + \Omega(\varphi)$ where $\Omega(\varphi)$ is an odd function of φ. This bias can be experimentally determined by using the beam-reversal method, a rather time consuming technique which requires the physical exchange of the beam source and detector, or adopting the two-frequency separated oscillating fields technique as suggested in [3]. Therefore a theoretical evaluation of the cavity phase shift appears advisable in order to determine its magnitude and to make clear the dependence on geometrical parameters. The cavity

phase shift is analyzed here by considering the geometry of the experimental set-up of the Mg beam in operation, which could also easily be used for a Ca beam.

Since the phase shift depends on asymmetries in the resonator and in the atomic beam, different situations with perfectly collimated or divergent beams are investigated.

1. Operation and Model of Metastable Beam Frequency Standards

The operation principle of the Mg frequency standard based on a fine structure transition within the $^3P_{0,1,2}$ metastable triplet, described in [1], is sketched in Fig. 1.

Part of ground-state atoms, coming out of an oven at 520 °C, are excited to the metastable triplet by means of electron collisions. The spontaneous decay rate γ^{-1} of $^3P_1$ to the ground state, of the order of milliseconds, introduces a natural population difference between metastable levels and at the same time suggests an efficient detection technique. In the experimental set-up, a signal is obtained by repopulating the $^3P_1$ level with a radiation resonant with the $^3P_0 - {}^3P_1$ $\Delta m_j = 0$ transition and by detecting the corresponding fluorescence increase with a photomultiplier.

A narrow linewidth is achieved by means of the Ramsey interrogation method: two interaction regions, with a free evolution of length L in between, produce interference fringes whose experimental observation is reported in [1]. The natural decay process, which is fundamental for preparing a population difference (length D) and for detecting the transition, in the free evolution region (length L) may contribute in a significant way to the final observation according to the geometry of the experiment and to the $^3P_1$ lifetime.

According to the design used in the methane beam [4], a grid placed in the middle of the twice-folded resonator, with a $\lambda/2$ period and with $\lambda/4$ wide apertures, acts as a mechanical selector stopping atoms which, because of divergence, would cross regions where interactions should occur in opposite phases. This geometrical sampling is to be considered in the following evaluations together with the consideration that all the physical phenomena involved in the beam operation, i.e. production of metastable atoms, population difference and detection, transition excitation, are velocity dependent.

Useful expressions to evaluate the cavity phase shift are obtained through the Maxwell-Bloch equations applied to the density matrix formalism [5], in particular by using matrices of interaction ($\mathbf{M}_\mathrm{I}$), where $\gamma = 0$, and of decay ($\mathbf{M}_\mathrm{D}$) as defined in [6].

Since a frequency error very small compared to the Ramsey fringe linewidth is sought, i.e. the peak value of the transition probability occurs at a frequency Ω_1 very close to $\Omega = 0$, the approximation usually adopted [7] is to put $\Omega = 0$ in the $\mathbf{M}_\mathrm{I}$ matrices, attributing all the frequency dependence to the time of flight present in $\mathbf{M}_\mathrm{D}$. This means that integrations for point dependent fields can be performed exactly and expressions are correct under the assumption that the decay length L is much longer than the interaction zones.

According to the symbols used in [6], for each possible value $\mathbf{v}$ of the atom velocity vector and for each possible coordinate crossing point in the first region (the second is determined by the $\mathbf{v}$ value assumed), the final values of the Bloch vector $\mathbf{R}^{(f)}$ can be expressed through the initial values $\mathbf{R}^{(i)}$ in the

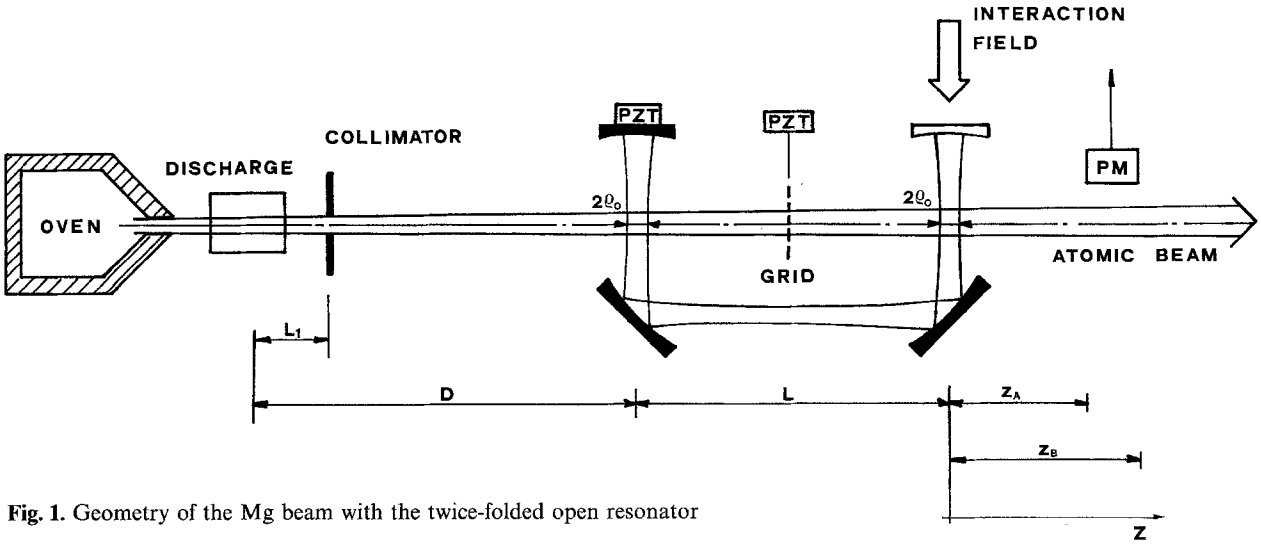

Fig. 1. Geometry of the Mg beam with the twice-folded open resonator

following way:

$$\mathbf{R}^{(f)} = \mathbf{M}_{I2}\mathbf{M}_D\mathbf{M}_{I1}R^{(i)}. \quad (1)$$

The subscripts 1 and 2 in $\mathbf{M}_I$ refer to the first and second interrogations respectively. The four components of $\mathbf{R}$ are directly related to the real (R_1) and imaginary (R_2) parts of atom polarization and to population difference (R_3) and sum (R_4). Their specific expressions, through the density matrix elements ϱ_{ij}, are

$$R_1 = \varrho_{12}e^{-i(\omega t+\psi)} + \varrho_{12}^* e^{i(\omega t+\psi)},$$

$$R_2 = i[\varrho_{12}e^{-i(\omega t+\psi)} - \varrho_{12}^* e^{i(\omega t+\psi)}],$$

$$R_3 = \varrho_{22} - \varrho_{11},$$

$$R_4 = \varrho_{22} + \varrho_{11},$$

where ψ is the phase of the electromagnetic field.

The initial values $\mathbf{R}^{(i)}$ can be obtained via the decay process between the source of metastable atoms and the first interaction. The general assumption $R_1^{(i)} = R_2^{(i)} = 0$ is made in the following. The signal at the detector is proportional to the variation $\Delta[R_3^{(f)} + R_4^{(f)}] = (R_3^{(f)} + R_4^{(f)})_{\omega_R} - (R_3^{(f)} + R_4^{(f)})_{\omega_R = 0}$ [6], between z_A and z_B, ω_R being the coordinate dependent Rabi angular frequency. Due to decay, the evolution of $(R_3 + R_4)$ with z between z_A and z_B is

$$R_3 + R_4 = (R_3^{(f)} + R_4^{(f)})e^{-\gamma z/v}. \quad (2)$$

A few different situations are considered in the following sections to evaluate the phase shift error. At the beginning an atomic beam without divergence in the plane (z, ξ) is assumed (see Fig. 2). If the beam velocity has only the v_z component, that is the crossings between beam and propagation axes ξ_1 and ξ_2 are orthogonal, different cases, of perfect alignment and of small misalignments between grid and standing waves, are analyzed. Perfect collimation requires a beam very narrow along ξ, as a consequence the signal-to-noise ratio is reduced, but in the former case the phase shift is zero to this order of approximation.

Subsequently a collimated beam with a small inclination is considered between z axis and $\mathbf{v}$ vector in the plane (z, ξ). This is a premise to the last case of phase shift with a divergent beam. The analysis is performed on the general assumption of point dependent fields, that is $\omega_R = \omega_R(\xi, y, z)$.

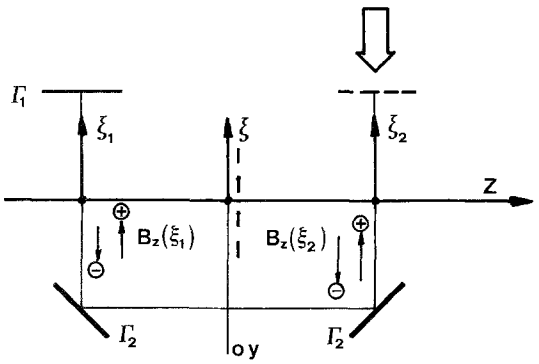

Fig. 2. Coordinate system used for the electromagnetic field distributions in the folded resonator

2. Phase Difference in the Optical Resonator

In the experimental set-up of the Mg beam, the twice-folded open resonator used is shown in Fig. 2. The Q factor is mainly determined by mirror losses and by coupling through the semitransparent metal mesh, whereas contributions from diffraction losses are negligible. According to this assumption the rf mangetic field B_z, parallel to the quantization axis z, can be expressed in the two regions with axes ξ_1 and ξ_2 by means of two counterpropagating fields labeled with superscripts + and − according to the direction of the propagation vector with respect to the $\xi_{1,2}$ axes. By introducing the electric field reflection coefficients $\Gamma_{1,2}$, considering in a first approximation the field as a superposition of counterpropagating plane waves, the expressions for B_z on the propagation axes, under resonance conditions are:

$$B_z(\xi_1) = B_z^+(\xi_1) + B_z^-(\xi_1) = B_p|\Gamma_2|^2\left[\cos\beta\xi_1\cos\omega t - \frac{1-|\Gamma_1|}{2}\cos(\omega t+\beta\xi_1)\right], \quad (3a)$$

$$B_z(\xi_2) = B_z^+(\xi_2) + B_z^-(\xi_2) = B_p\left[\cos\beta\xi_2\cos\omega t - \frac{1-|\Gamma_1\Gamma_2^4|}{2}\cos(\omega t-\beta\xi_2)\right], \quad (3b)$$

where equal phases and maxima of standing waves were imposed at $\xi_1 = \xi_2 = 0$. In an ideal situation the straight line between these two points is parallel to the atomic beam direction which is the quantization axis z as well. In expressions (3a) and (3b) $\beta = 2\pi/\lambda$ and $B_p/2$ is the amplitude of B_2^+ wave at $\xi_2 = 0$. The rf field phase variations δ with ξ_1 and ξ_2 are easily obtained from (3a) and (3b).

$$\delta(\xi_1) = -\arctan\left[\frac{1-|\Gamma_1|}{1+|\Gamma_1|}\tan\beta\xi_1\right] + \alpha_{n1}\pi, \quad (4a)$$

$$\delta(\xi_2) = \arctan\left[\frac{1-|\Gamma_1\Gamma_2^4|}{1+|\Gamma_1\Gamma_2^4|}\tan\beta\xi_2\right] + \alpha_{n2}\pi, \quad (4b)$$

where the coefficient $\alpha_{n1,2}$ is zero when $\beta\xi_{1,2}$ belongs to an interval $-\frac{\pi}{2}\rightarrow+\frac{\pi}{2}$ around $2n\pi$ and is 1 when the interval $-\frac{\pi}{2}\rightarrow+\frac{\pi}{2}$ is around $(2n+1)\pi$.

When the skin effect is predominant the reflection coefficient of metal mirrors can be expressed as

$$\Gamma_1=-\frac{1-(1+\mathrm{i})r_1}{1+(1+\mathrm{i})r_1}\quad\text{with}\quad r_1\equiv r_m^{\perp}=\sqrt{\frac{\omega\varepsilon_0}{2\sigma_1}},$$

$$\Gamma_2=-\frac{1-(1+\mathrm{i})r_2}{1+(1+\mathrm{i})r_2}\quad\text{with}\quad r_2=\frac{1}{2}\sqrt{\frac{\omega\varepsilon_0}{\sigma_2}},$$

where ε_0 is the vacuum permittivity, σ_1 and σ_2 are metal conductivities and the change in the numerical factor in r_2 comes from the incidence at 45° on the two equal mirrors. In this case, the approximation $|\Gamma|\simeq 1-2r$ leads to

$$\delta(\xi_1)\simeq-\arctan[r_1\tan\beta\xi_1]+\alpha_{n1}\pi, \tag{5a}$$

$$\delta(\xi_2)\simeq\arctan[(r_1+4r_2)\tan\beta\xi_2]+\alpha_{n2}\pi. \tag{5b}$$

The phase shift φ between the two regions is $\varphi=\delta(\xi_2)-\delta(\xi_1)$ with $\delta(\xi_1)$ and $\delta(\xi_2)$ given by (4) or (5).

The phase difference between points lying on the axes ξ_2 and ξ_1 is represented by the expression

$$\varphi(\xi_2,\xi_1)=\arctan(K_2\tan\beta\xi_2)+\arctan(K_1\tan\beta\xi_1)+(\alpha_{n2}-\alpha_{n1})\pi, \tag{6}$$

where K_1 and K_2 are very small coefficients obtained in a straightforward way from the expressions (4).

3. A General Expression of the Phase-Shift Error

The phase-shift expression given in [8] is here made general to include the ω_R dependence on the coordinates and the decay process of one metastable level ($^3P_1$) with rate γ^{-1}.

Following [6, Eq. (A5)], the decay matrix $\mathbf{M}_D$ is:

$$\mathbf{M}_D=\begin{vmatrix} d_{11} & d_{12} & 0 & 0\\ d_{21} & d_{22} & 0 & 0\\ 0 & 0 & d_{33} & d_{34}\\ 0 & 0 & d_{43} & d_{44}\end{vmatrix}, \tag{7}$$

where

$$d_{11}=d_{22}=\mathrm{e}^{-\gamma L/2v_z}\cos\left(\Omega\frac{L}{v_z}+\varphi\right),$$

$$d_{21}=-d_{12}=\mathrm{e}^{-\gamma L/2v_z}\sin\left(\Omega\frac{L}{v_z}+\varphi\right),$$

$$d_{33}=d_{44}=(1+\mathrm{e}^{-\gamma L/v_z})/2,$$

$$d_{34}=d_{43}=-(1-\mathrm{e}^{-\gamma L/v_z})/2$$

and φ, given by expression (6), takes into account the phase difference between the two zones.

The specific expressions for interaction matrices are reported in the following sections; however, due to the condition $\Omega=0$, their general form is [6, Eqs. (A7, A8)]:

$$\mathbf{M}_I=\begin{vmatrix} 1 & 0 & 0 & 0\\ 0 & i_{\vartheta 22} & i_{\vartheta 23} & 0\\ 0 & i_{\vartheta 32} & i_{\vartheta 33} & 0\\ 0 & 0 & 0 & 1\end{vmatrix} \tag{8}$$

with $i^{(j)}_{\vartheta 22}=i^{(j)}_{\vartheta 33}$ and $i^{(j)}_{\vartheta 32}=-i^{(j)}_{\vartheta 23}$, j assuming the values 1 or 2 according to the interaction zone considered, and ϑ is the inclination angle with z of an atomic trajectory in the (z,ξ) plane.

To improve the previous approximations, that is the identification in the matrix $\mathbf{M}_D$ elements of the free evolution length L with the distance between the two gaussian beams and the condition $\Omega=0$ in the matrix $\mathbf{M}_I$ elements, respectively, the Rosen-Zener conjecture can be used [9, 10]. The latter is an approximate extension of the only known solution of the two-level problem with a non-constant interaction field, with envelope $f(t)=\mathrm{sech}(t/\tau_0)$, to the case of a field envelope function $g(t)$, continuous with its first derivative and Fourier-transformable. The transition probability is then proportional to $\left|\int_{-\infty}^{+\infty} g(t)\mathrm{e}^{\mathrm{i}\Omega t}dt\right|^2$.

By applying this evaluation method to the double interaction with gaussian beams, a linewidth value is found which, when compared to that obtained through the use of matrices $\mathbf{M}_D$ and $\mathbf{M}_I$, suggests the substitution of L with the more appropriate value

$$L_e=\sqrt{L^2+\frac{\pi}{4}(2\varrho_0)^2}$$

ϱ_0 being the gaussian beam radius at e^{-1} of power.

Introducing in (1) expressions (7) and (8) with the specified initial conditions $R_1^{(i)}=R_2^{(i)}=0$ we get

$$R_3^{(f)}=i^{(2)}_{\vartheta 32}i^{(1)}_{\vartheta 23}d_{22}R_3^{(i)}+i^{(2)}_{\vartheta 33}[d_{33}i^{(1)}_{\vartheta 33}R_3^{(i)}+d_{34}R_4^{(i)}], \tag{9}$$

with

$$R_4^{(f)}=d_{43}i^{(1)}_{\vartheta 33}R_3^{(i)}+d_{44}R_4^{(i)}, \tag{10}$$

$$R_3^{(i)}=-1/2(1-\mathrm{e}^{-\gamma D/v_z})$$

and

$$R_4^{(i)}=+1/2(1+\mathrm{e}^{-\gamma D/v_z}).$$

The average probability $\langle P(\Omega)\rangle$ to detect the transition is proportional to

$$\langle P(\Omega)\rangle\propto\int_{\vartheta}\int_{\Sigma}\int_{v} f(v)\Phi(\vartheta)\Delta[R_3^{(f)}+R_4^{(f)}]\times(\mathrm{e}^{-\gamma z_A/v_z}-\mathrm{e}^{-\gamma z_B/v_z})d\sigma d\vartheta dv, \tag{11}$$

where $f(v)$ is the metastable atom velocity distribution at the end of the electric discharge and $\Phi(\vartheta)$ is the angle

dependent flux density. The integrations are carried out over the velocity distribution and the ensemble of coordinates $\sigma(\xi_{1,2}, y)$ ranging over the surface Σ with correlations between first and second Ramsey zones coordinates according to the allowed trajectories. The solution looked for is the value Ω_1 for which $d\langle P(\Omega)\rangle/d\Omega=0$. In expression (11) only the matrix element d_{22} coming from (9) is Ω dependent through $\cos(\Omega L_e/v_z+\varphi)$, therefore the cavity phase-shift bias must satisfy the equation

$$\int_v\int_\Sigma\int_\vartheta F(v)\Phi(\vartheta)\frac{L_e}{v}I(v,\sigma,\vartheta)\times\left[\Omega_1\frac{L_e}{v}\cos\varphi+\sin\varphi\right]dvd\vartheta d\sigma=0, \tag{12}$$

where it has been assumed that $\Omega_1 L_e/v_z\ll 1$,

$$F(v)=f(v)e^{-\gamma(L+D)/2v_z}\times\sinh(\gamma D/2v_z)(e^{-\gamma z_A/v_z}-e^{-\gamma z_B/v_z})$$

and $I(v,\sigma,\vartheta)=i^{(2)}_{32}i^{(1)}_{23}$.

The final expression follows

$$\frac{\Omega_1}{\omega_0}\simeq-\frac{1}{\omega_0 L_e}\frac{\int_v\int_\vartheta\int_\Sigma\Phi(\vartheta)\frac{F(v)}{v}I(v,\sigma,\vartheta)\sin\varphi dvd\sigma d\vartheta}{\int_v\int_\vartheta\int_\Sigma\Phi(\vartheta)\frac{F(v)}{v^2}I(v,\sigma,\vartheta)\cos\varphi dvd\sigma d\vartheta}. \tag{13}$$

It can be remarked that, in many cases, φ assumes only values very close to 0 or π, and therefore suitable approximations are $\sin\varphi=\pm\varphi$ and $\cos\varphi=\pm 1$ respectively. To avoid misunderstandings because of the two possible approximations the notation $\sin\varphi$ and $\cos\varphi$ is maintained when necessary. Moreover, according to (6), for some trajectories this assumption does not hold.

Due to the small ϑ values allowed by the collimators, significant variations of Φ with ϑ were not experimentally found, therefore from now on $\Phi(\phi)$ is assumed a constant and it is omitted in what follows.

For a metastable Mg beam an expression of the velocity distribution $f(v)$ has been obtained in [11] analyzing the case of metastabilization through atom-electron collisions

$$f(v)=A(v/\alpha)^{\bar\gamma}e^{-HI/v-v^2/\alpha^2}\sinh(KI/v),$$

where

A = normalization constant;

α = the most probable velocity in the oven;

$\bar\gamma$ = positive number higher than 3. It takes into account the elastic collision effect;

I = discharge current;

H and K are constants dependent on the excitation and deexcitation cross-sections of Mg and on the discharge geometry.

4. Orthogonal Interaction with a Collimated Atomic Beam

In this case

$$i^{(j)}_{22}=i^{(j)}_{33}=\cos[\zeta(\beta\xi_j)],$$

$$i^{(j)}_{32}=-i^{(j)}_{23}=\sin[\zeta(\beta\xi_j)],$$

where, according to (A.10) of [6], ζ takes into account the field shape seen by the atom and, in particular, for a gaussian electromagnetic beam

$$\zeta=e^{-y^2/2\varrho_0^2}\chi/v\cos\beta\xi_j$$

being $\chi=\sqrt{2\pi}\varrho_0\omega_{R0}$, $\omega_{R0}=\mu B_p/\hbar$ and μ the transition dipole moment which, in the Russel-Sounders coupling, is $\sqrt{2/3}$ times the Bohr magneton.

For the orthogonal interaction of Fig. 2, $\xi_1=\xi_2=\xi$ and, if the atomic beam engages an integer number M of slits of the grid centered at $\xi=i\lambda/2$, i being a negative

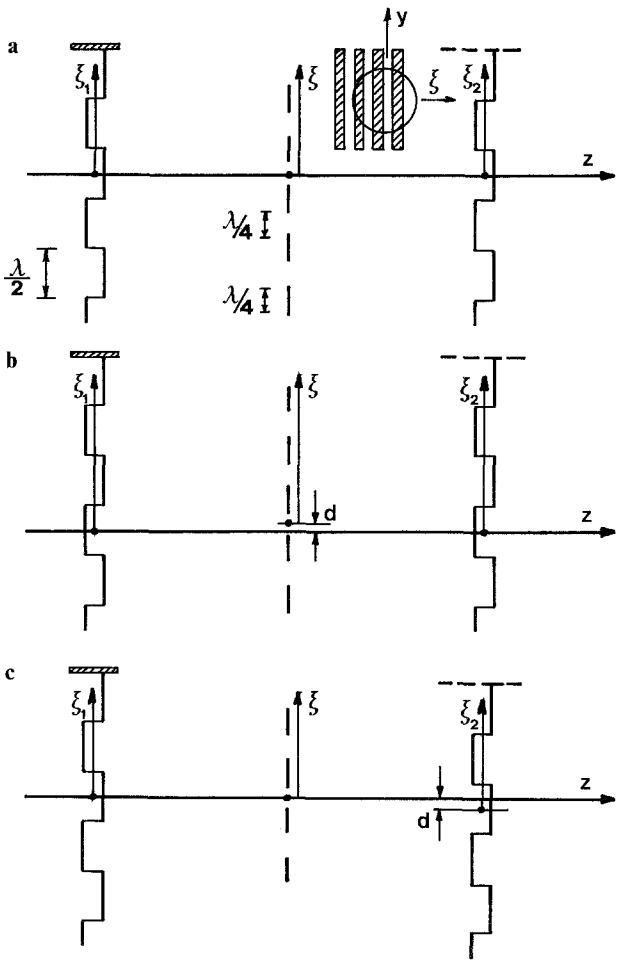

Fig. 3a–c. Different asymmetries in an orthogonal interaction of a collimated beam. **a** Slits are not homogeneously filled with atoms. **b** The grid is not aligned with the standing waves. **c** A standing wave is not aligned with the grid and the other standing wave. The steplike diagrams divide the $\xi_{1,2}$ axes in zones where phases of perfect standing waves are 0 or π respectively

or positive integer, the net result of (13) is $\Omega_1 = 0$ due to the odd and even dependence on ξ of φ and $(i_{32}^{(2)} \cdot i_{12}^{(1)})$ respectively.

On the other hand, if not all slits are filled with the atom flow (Fig. 3a), an unbalanced term comes out from (13) and the maximum error is

$$\frac{\Omega'_{1M}}{\omega_0} \simeq \mp \frac{K_2 + K_1}{2M\omega_0 L_e} \times \frac{\int_0^\infty F(v)\frac{dv}{v}\int_0^{\varrho_0} dy \int_0^{\pi/4} \sin^2\zeta(\beta\xi)\tan\beta\xi d(\beta\xi)}{\int_0^\infty F(v)\frac{dv}{v^2}\int_0^{\varrho_0} dy \int_0^{\pi/4} \sin^2\zeta(\beta\xi)d(\beta\xi)}, \tag{14}$$

where $\varphi(\beta\xi) \simeq (K_1 + K_2)\tan\beta\xi$ is obtained from (6) with $\xi_1 = \xi_2 = \xi$ and the integration limit ϱ_0 follows from a suitable approximation of the atomic beam cross-section dimension in the two interaction zones. By moving the grid it is possible to evaluate the total variation.

This error can be reduced by adjusting the width of the semitransparent portion of the grid to be sure that all the slits are symmetrically filled with atoms.

If there is a misalignment d between grid and standing waves (Fig. 3b), then $\xi_1 = \xi_2 = \xi + d$ and the frequency error is

$$\frac{\Omega''_1}{\omega_0} \simeq -\frac{1}{\omega_0 L_e} \times \frac{\int_0^\infty F(v)\frac{dv}{v}\int_0^{\varrho_0} dy \int_{\pi/4-\beta d}^{\pi/4+\beta d} \zeta(u)\sin\varphi(u)du}{\int_0^\infty F(v)\frac{dv}{v^2}\int_0^{\varrho_0} dy \int_{-\pi/4+\beta d}^{\pi/4+\beta d} \sin^2\zeta(u)\cos\varphi(u)du}, \tag{15a}$$

where $u = \beta\xi_1$. If $d = \varepsilon \ll 1/\beta$

$$\frac{\Omega''_1}{\omega_0} \simeq -\frac{K_2 + K_1}{cL_e}\varepsilon \times \frac{\int_0^\infty F(v)\frac{dv}{v}\int_0^{\varrho_0} dy \sin^2(e^{-y^2/2\varrho_0^2}\chi/\sqrt{2}v)}{\int_0^\infty F(v)\frac{dv}{v^2}\int_0^{\varrho_0} dy \int_0^{\pi/4} \sin^2\zeta(u)du}, \tag{15b}$$

where c is the velocity of light.

If a misalignment d occurs between standing waves maxima, e.g. $\xi_1 = \xi_2 + d$ (Fig. 3c), leaving $\xi = \xi_1$, the expression (13) yields

$$\frac{\Omega'''_1}{\omega_0} \simeq -\frac{1}{\omega_0 L_e} \frac{\int_0^\infty F(u)\frac{dv}{v}\int_0^{\varrho_0} dy \int_{-\pi/4}^{\pi/4} i_{32}(\xi_1 - d)i_{23}(\xi_1)\sin\varphi(\xi_1 - d, \xi_1)d(\beta\xi_1)}{\int_0^\infty F(v)\frac{dv}{v^2}\int_0^{\varrho_0} dy \int_{-\pi/4}^{\pi/4} i_{32}(\xi_1 - d)i_{23}(\xi_1)\cos\varphi(\xi_1 - d, \xi_1)d(\beta\xi_1)}. \tag{16a}$$

Even and odd (non-contributing) functions of $\beta\xi$ under integration in (16a) can be easily separated. A simplified expression is possible for $d = \varepsilon$ in the case $\beta\varepsilon\chi/v \ll 1$

$$\frac{\Omega'''_1}{\omega_0} \simeq -\frac{\varepsilon}{cL_e} \frac{\int_0^\infty F(v)\frac{dv}{v}\int_0^{\varrho_0} dy \int_{-\pi/4}^{\pi/4}\left[-K_2\frac{\sin^2(C\cos u)}{\cos^2 u} + \frac{K_1 + K_2}{2}C\frac{\sin^2 u}{\cos u}\sin(2C\cos u)\right]du}{\int_0^\infty F(v)\frac{dv}{v^2}\int_0^{\varrho_0} dy \int_0^{\pi/4} \sin^2(C\cos u)du} \tag{16b}$$

being $C = (\chi/v)e^{-y^2/2\varrho_0^2}$.

This expression was compared with numerical integration of (16a) and it turned out to be a suitable approximation also when $\beta\varepsilon\chi/v \lesssim 1$.

In the numerical computations the figures listed in Table 1 have been used. These correspond to the experimental realization of the Mg beam. Diagrams obtained from expressions (15b) and (16a) are reported in Fig. 4 as a function of χ, which is proportional to the standing wave amplitude inside the resonator. Both the grid and the second standing wave are supposed to be shifted by $d = 10\,\mu m$ from their ideal position separately. Curves b) and c) refer to grid and standing wave movement respectively. The value $\chi_{OPT} = 1581$ m/s which normalizes the horizontal axis comes from [6], where the case of a perfectly collimated beam was considered, taking into account the actual velocity distribution and the experimental parameters. The relative phase-shift error in a collimated beam is evaluated from Fig. 4 of the order of a few units in 10^{13} with the possibility of some reduction because of the even dependence on the misalignment d.

Table 1. Parameter values used in the numerical computations

Parameter	Value	Parameter	Value
D	1.15 m	γ^{-1}	4.6×10^{-3} s
L	0.3 m	α	736 m s^{-1}
L_1	0.27 m	$\bar{\gamma}$	4
z_A	0.3 m	H	2200 m s^{-1} A^{-1}
z_B	0.5 m	K	1540 m s^{-1} A^{-1}
a	2×10^{-3} m	I	0.3 A
ϱ_0	8×10^{-3} m	$r_m^{\perp}$	10^{-3}
λ	498×10^{-6} m	χ_{OPT}	1581 m s^{-1}

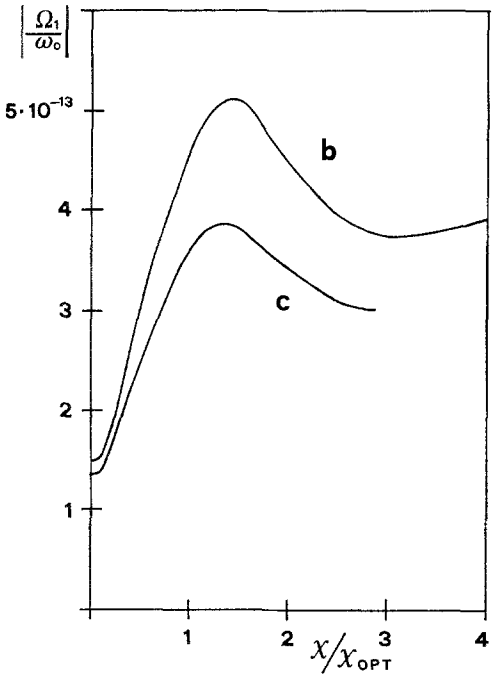

Fig. 4. Relative frequency error $|\Omega_1/\omega_0|$ for grid b and second standing wave c misalignments ($d=10$ μm) as a function of χ/χ_{OPT}

5. Non-orthogonal Interaction with a Collimated Atomic Beam

When a non-orthogonal interaction occurs, the travelling wave produces not only a cavity phase shift, but a first order Doppler effect as well. This latter effect is considered in a paper in preparation [12]. Here the analysis is concerned with the phase shift between points belonging to the coordinate axes ξ_1 and ξ_2 respectively.

If ϑ is the angle between the velocity vector $\mathbf{v}$ and z, following the previous notation for the Bloch vector $\mathbf{R}$, if the atoms cross a standing wave $g(z)\cos\beta\xi$ where $\xi(t)=\xi_0+v_\xi t$ and $z=z_0+v_z t$, the differential equation system for the components R_j is formally the same as written in [6, Eq. (A.7)].

In this case the $\mathbf{M}_I$ elements can be written as

$$i_{\vartheta 22}=i_{\vartheta 33}=\cos\zeta_\vartheta,\qquad i_{\vartheta 32}=-i_{\vartheta 23}=\sin\zeta_\vartheta, \tag{17}$$

where, for a gaussian beam,

$$\zeta_\vartheta=e^{-y^2/2\varrho_0^2}\frac{\chi}{v}\frac{e^{-\frac{1}{2}(\beta\varrho_0\tan\vartheta)^2}}{\cos\vartheta}\cos\beta\xi_0 \tag{18}$$

is an even function of ϑ and nearly constant if $\beta\varrho_0\tan\vartheta\ll1$.

In order to get a strong interaction with the Ramsey technique, the standing wave maxima and the slit centres have to be aligned. In this case the phase-shift expression is given by (6) after a suitable choice of origin for ξ_1 and ξ_2. Apart the small ϑ dependence of ζ_ϑ, present in expression (18), the bias evaluations given by (15a) and (16a) can be easily transferred to this case.

Another possibility can occur with standing wave and grid positions as shown in Fig. 5, the atomic beam having an inclination ϑ. Now atoms cross the two axes ξ_1 and ξ_2 at coordinates ξ_{10} and ξ_{20} given by

$$\xi_{10}=\xi-(L/2)\tan\vartheta,\qquad \xi_{20}=\xi+(L/2)\tan\vartheta \tag{19}$$

and the phase difference between ξ_{20} and ξ_{10}, linked by the trajectory (19), is

$$\begin{aligned}\varphi_\vartheta&=\arctan\{K_1\tan(\beta\xi_{10})\}\\&\quad+\arctan\{K_2\tan(\beta\xi_{20})\}+(\alpha_{n2}-\alpha_{n1})\pi\\&=\arctan\{K_1\tan[\beta(\xi-L/2\tan\vartheta)]\}\\&\quad+\arctan\{K_2\tan[\beta(\xi+L/2\tan\vartheta)]\}\\&\quad+(\alpha_{n2}-\alpha_{n1})\pi.\end{aligned} \tag{20}$$

For a given ξ value, φ_ϑ is periodic with ϑ; the period T_ϑ is given by $(\beta L/2)\tan T_\vartheta=\pi$, that is $T_\vartheta\simeq\lambda/L\simeq1.67$ mrad in the case examined.

For fully symmetric trajectories $\xi(t)=\xi_0+v_\xi t$ and $\xi(t)=-\xi_0-v_\xi t$, the product $i^{(2)}_{\vartheta 32}i^{(1)}_{\vartheta 23}$ is unchanged, whereas φ_ϑ has opposite values, apart the additive term $(\alpha_{n2}-\alpha_{n1})\pi$ which is unaltered; given a ϑ value, φ_ϑ is odd in ϑ only if $K_1=K_2$.

The phase-shift bias, assuming slits equally filled with atoms therefore gives a net result different from zero if $\vartheta\neq0$. The general expression in this case is

$$\frac{\Omega_{1\vartheta}}{\omega_0}=-\frac{1}{\omega_0 L_e}\frac{\int_0^\infty F(v)\frac{dv}{v}\int_0^{\varrho_0}dy\int_{-\pi/4}^{\pi/4}i_{\vartheta 32}(\beta\xi_{20})i_{\vartheta 23}(\beta\xi_{10})\sin\varphi_\vartheta d(\beta\xi)}{\int_0^\infty F(v)\frac{dv}{v^2}\int_0^{\varrho_0}dy\int_{-\pi/4}^{\pi/4}i_{\vartheta 32}(\beta\xi_{20})i_{\vartheta 23}(\beta\xi_{10})\cos\varphi_\vartheta d(\beta\xi)}, \tag{21}$$

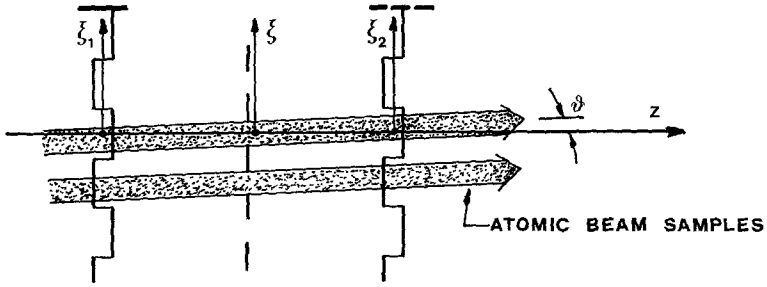

Fig. 5. A possible geometry of a non-orthogonal interaction of a collimated beam

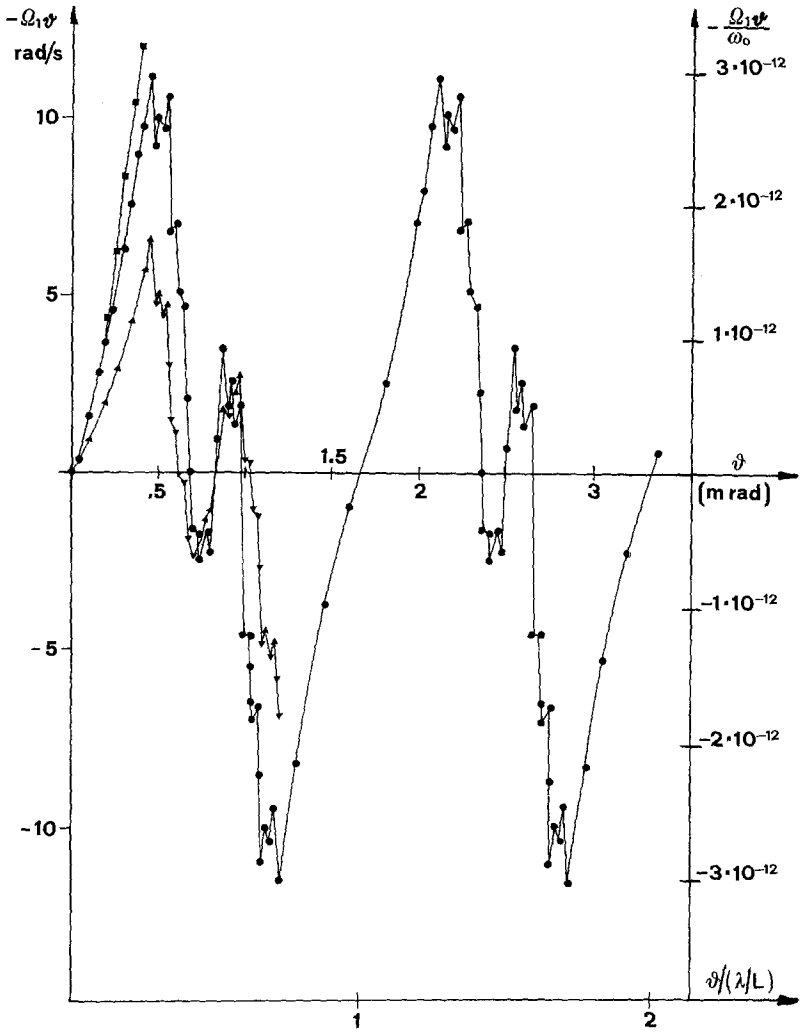

Fig. 6. Phase-shift error as a function of the inclination ϑ for a non-orthogonal interaction as in Fig. 5. ϑ scale in units of λ/L is also shown. ▲ $\chi=0.5\,\chi_{OPT}$, ● $\chi=\chi_{OPT}$, ■ $\chi=1.5\,\chi_{OPT}$

where the relationships between ξ_{20}, ξ_{10}, and ξ are given in (19).

Expression (21) with the integration limits on $\beta\xi$ indicated is a quasi-periodic and odd function of ϑ if $\vartheta \ll 1$ and ζ_ϑ can be taken as nearly independent of ϑ. The two-zone distance L is not only explicit in the factor L_e, but terms in $\xi \pm L/2 \tan\vartheta$ are also in the integrands, namely in $i_{\vartheta 32}$, $i_{\vartheta 23}$, and φ_ϑ. This effect cannot be discussed directly. Moreover it must be pointed out that, for atoms crossing the same slit, part interact with equal phase, part with opposite phase fields when

$$\lambda(n/2+1/8) < (\beta L/2)\tan\vartheta < (n/2+3/8)\lambda .$$

In Fig. 6 the diagram of Ω_{10}/ω_0 is presented as a function of ϑ having χ/χ_{OPT} as a parameter. At varying ϑ, with period λ/L, when the inclination approaches $\lambda/4L$ there are many atoms which suffer a large phase shift and, moreover, cross standing waves of opposite

phases. The pattern of $\Omega_{1\vartheta}/\omega_0$ is then rather irregular in the region $\lambda/4L \leqq \vartheta \leqq (3/4)\lambda/L$.

A computed evaluation of (21) for different L values has shown that the bias $\Omega_{1\vartheta}/\omega_0$ is proportional to $1/L$, the ratio between integrals being independent of L.

With reference to the experimental case when a symmetry exists around the z axis and the slits are centered at $\xi = i\lambda/2$, if the grid is displaced by d, each slit is crossed by atoms seeing a phase shift which cannot be compensated. The bias is

$$\frac{\Omega'_{1D}}{\omega_0} \simeq -\frac{1}{\omega_0 L_e} \frac{\int_0^\infty F(v)\frac{dv}{v}\int_0^{\varrho_0} dy \int_{\pi/4-\delta d}^{\pi/4+\beta d} du \sum_i \int_{\vartheta_{1i}}^{\vartheta_{ui}} d\vartheta i_{\vartheta 32}(\xi_{20}) i_{\vartheta 23}(\xi_{10}) \sin\varphi_\vartheta(\xi_{20},\xi_{10})}{\int_0^\infty F(v)\frac{dv}{v^2}\int_0^{\varrho_0} dy \int_{-\pi/4+\beta d}^{\pi/4+\beta d} du \sum_i \int_{\vartheta_{1i}}^{\vartheta_{ui}} d\vartheta i_{\vartheta 32}(\xi_{20}) i_{\vartheta 23}(\xi_{10}) \cos\varphi(\xi_{20},\xi_{10})}, \tag{22}$$

6. Interaction with a Divergent Beam

According to the results of the preceding sections, when a divergent beam interacts with two standing waves, the phase-shift bias is compensated overall if a perfect geometrical symmetry exists with respect to the z axis. Only asymmetries in the beam flux density Φ or in the relative positions of standing waves, grid and beam can produce phase shifts which, when integrated, do not average to zero.

In the case of the Mg beam considered, the full divergence is about 10 mrad, but the full aperture Θ of the atom flows across a slit is nearly ξ-independent, that is

$$\Theta \simeq 2a/(D - L_1 + L/2),$$

where $2a$ is the diaphragm aperture (Fig. 1).

The corresponding upper and lower limit values for $\vartheta(\xi)$ are respectively

$$\vartheta_u = (\xi + a)/(D - L_1 + L/2)$$

and

$$\vartheta_l = (\xi - a)/(D - L_1 + L/2).$$

In the experimental situation described $\Theta \simeq 4 \times 10^{-3}$ and the range Δ over ξ_1 or ξ_2 spanned by atoms crossing a single slit is $\Delta \simeq (L/2)\Theta + \lambda/4 \simeq 3\lambda/2$.

where expressions (19) hold between $\xi = u/\beta$ and the coordinates ξ_{20} and ξ_{10} through ϑ, the expressions $i_{\vartheta 32}$, $i_{\vartheta 23}$, and φ_ϑ are independent of i, depending only on ξ, but the integration limits along ϑ depend on i; in fact

$$\vartheta_{ui} \simeq \frac{i\frac{\lambda}{2} + \frac{\lambda}{8} + d + a}{D - L_1 + L/2}, \quad \begin{matrix} d > 0 \\ \vartheta'_{ui} = \vartheta_{\widehat{ui}}, \\ d < 0 \end{matrix}$$

$$\vartheta'_{ui} = \frac{i\frac{\lambda}{2} - \frac{\lambda}{8} - d + a}{D - D_1 + L/2},$$

$$\vartheta_{li} \simeq \frac{i\frac{\lambda}{2} - \frac{\lambda}{8} + d - a}{D - L_1 + L/2}, \quad \vartheta'_{li} = \frac{i\frac{\lambda}{2} + \frac{\lambda}{8} - d - a}{D - L_1 + L/2}, \quad \vartheta'_{li} = \vartheta_{ii}$$

with the exception of the extreme slits where the limits are imposed by the atomic beam dimensions. Figure 7 shows the computed dependences of Ω'_{1D}/ω_0 on d, having χ/χ_{OPT} as a parameter. For a displacement $d = \lambda/2$, the geometry of the experiment reproduces itself exactly, whereas for $d = \lambda/4$ the observed Ramsey fringe is inverted [1], the contrast and the phase shift being practically the same although different atom paths are sampled.

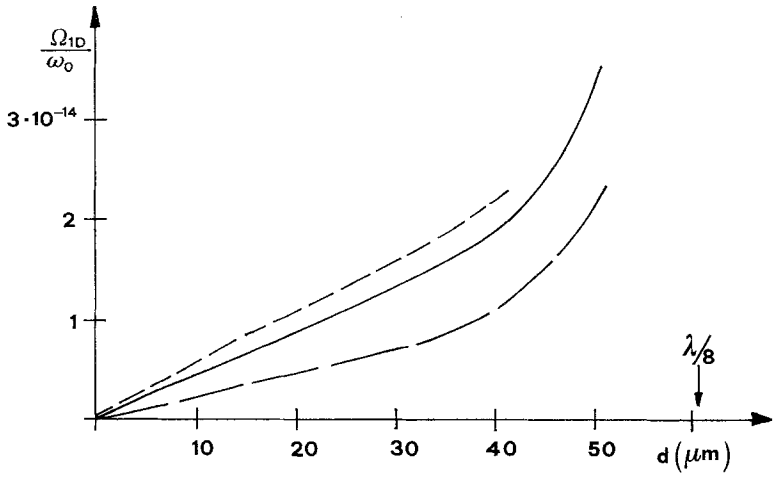

Fig. 7. Phase-shift error Ω_{1D}/ω_0 as a function of the grid displacement d for an orthogonal divergent beam. — — — $\chi = 0.5\,\chi_{OPT}$, ——— $\chi = \chi_{OPT}$, ----- $\chi = 1.5\,\chi_{OPT}$

If these evaluations are compared with those of a collimated beam, the beam divergence appears to play an important role in reducing the frequency bias by averaging contributions corresponding to different paths. In fact, a reduction of a factor of nearly 100 is obtained, comparing Fig. 4 with Fig. 7, for the same power level at a grid displacement of 10 μm.

If the asymmetry consists of a small angle ϑ_0 between the beam axis and the z axis, an expression similar to (22) can be introduced with the following new integration limits both at numerator and denominator:

$$\vartheta_{li}+\vartheta_0 \quad \text{and} \quad \vartheta_{ui}+\vartheta_0 \quad \text{for } \vartheta,$$
$$-\pi/4+\beta d \quad \text{and} \quad \pi/4+\beta d \quad \text{for } u$$

provided the origins of ξ_1, ξ, and ξ_2 are moved to keep standing wave maxima and slit centres on a straight line with inclination ϑ_0.

Accordingly the following expressions hold:

$$\zeta_{\vartheta}^{\left(\frac{1}{2}\right)} = e^{-y^2/2\varrho_0^2} \frac{\chi}{v} \frac{e^{-\frac{1}{2}(\beta\varrho_0 \tan\vartheta)^2}}{\cos\vartheta} \times \cos\left[u \mp \beta\frac{L}{2}(\tan\vartheta - \tan\vartheta_0)\right], \tag{23}$$

$$\varphi_0 = \arctan\left\{K_1 \tan\left[u - \frac{\beta L}{2}(\tan\vartheta - \tan\vartheta_0)\right]\right\} + \arctan\left\{K_2 \tan\left[u + \frac{\beta L}{2}(\tan\vartheta - \tan\vartheta_0)\right]\right\}. \tag{24}$$

By introducing (23) and (24) with the appropriate integration limits in (22) an expression for $\Omega_{1D}(\vartheta_0)/\omega_0$ is obtained. It is straightforward to notice that the ϑ_0 dependence is odd and different from zero, even for $d=0$. As u is centered around zero, very strong variations in φ_ϑ are to be expected when $\beta(L/2)\tan\vartheta_0 \simeq \pi/2$ that is $\vartheta_0 \simeq \lambda/2L$, for $K_2 \neq K_1$. This is shown in Fig. 8 where the computed values of $\Omega_{1D}(\vartheta_0)/\omega_0$ in the case $\chi=\chi_{OPT}$ are reported. The averaging effect due to divergence is again rather strong and the relative frequency error can be limited to the level of units in 10^{14} if proper checks of suitable experimental conditions are performed to avoid ϑ_0 positions around $\lambda/2L$. When $d \neq 0$, far from this ϑ_0 value, the effect of a 10 μm displacement should be limited to the 10^{-14} level, as it turns out from Fig. 7.

As far as the dependence of frequency uncertainty on the field amplitude is concerned, it is likely that divergence imposes, for the maximum output signal, a χ value higher than the χ_{OPT} used in these computations. An appropriate value should occur between χ_{OPT} and $1.5\,\chi_{OPT}$, but the diagrams of Figs. 4 and 7 show that the error increase is not substantial. Accordingly the phase-shift error for the described experimental set-up of the Mg beam should be lower than 10^{-13} even with a two-zone distance of only 0.3 m.

From the experimental point of view the odd dependence of the error on displacements and inclinations could be exploited for a better definition of the operation condition close to the ideal case. Moreover the beam reversal technique, which is also useful to

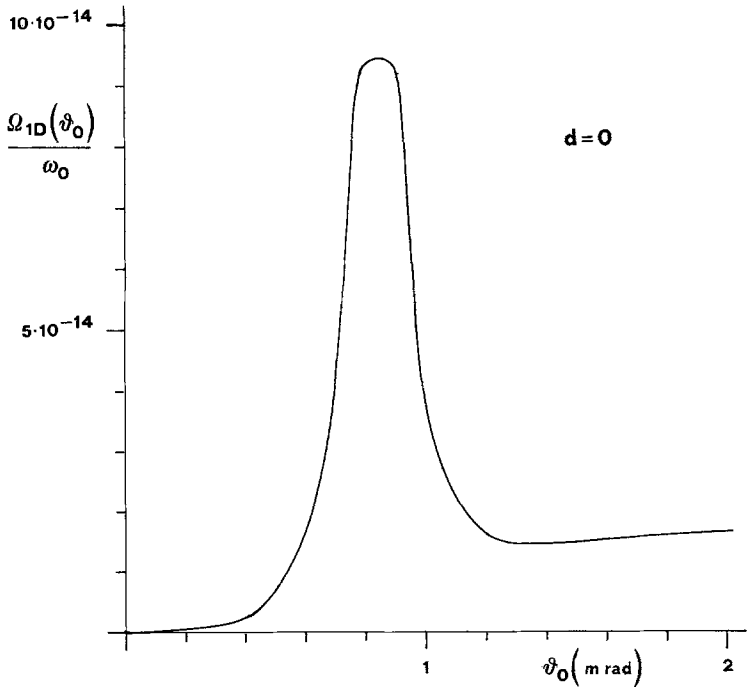

Fig. 8. Relative frequency error $\Omega_{1D}(\vartheta_0)/\omega_0$ for a divergent beam with inclination ϑ_0 with respect to the z axis. The diagram refers to $\chi=\chi_{OPT}$ with the grid centered for maximum signal ($d=0$)

reduce the residual first order Doppler effect, could be performed with two counterpropagating atomic beams whose alignment could be easily checked by optical methods due to the absence of selecting magnets in the structure.

7. Conclusions

In atomic beams with the transverse dimensions much larger than the wavelength, specific problems arise when determining the Ramsey cavity phase-shift effect on the resonance frequency; this is of interest in submillimetric standards based on Mg or Ca atoms or on molecular transitions. Moreover, determination of fundamental constants through millimetric transitions of Rydberg atoms should face similar problems. A rather general analysis of the effect has been performed whereas computations were limited to the experimental realization of an Mg standard. The beam divergence yields atom trajectories whose phase shift between the two zones assumes very widespread values of opposite sign as well. As a consequence, a strong averaging effect occurs which reduces the frequency error to a level lower than in the case of a collimated beam.

References

1. A. Godone, E. Bava, C. Novero: Metrologia **24**, 133 (1987)
2. N. Ramsey: *Molecular Beams* (Clarendon, Oxford 1986)
3. R.M. Garwey, H.W. Hellwig, S. Jarvis, Jr., D.J. Wineland: IEEE Trans. IM-**27**, 349 (1978)
4. G. Kramer: J. Opt. Soc. Am. **68**, 1634 (1978)
5. M. Sargent III, M.O. Scully, W.E. Lamb, Jr.: *Laser Physics* (Addison-Wesley, London 1974)
6. E. Bava, A. Godone, G. Rietto: Appl. Phys. B **41**, 187 (1986)
7. C. Audoin: *Metrology and Fundamental Constants* (North-Holland, Amsterdam 1980)
8. N.F. Ramsey, H.B. Silsbee: Phys. Rev. **84**, 506 (1951)
9. N. Rosen, C. Zener: Phys. Rev. **40**, 502 (1932)
10. R.T. Robiscoe: Phys. Rev. A **17**, 247 (1978)
11. G. Giusfredi, A. Godone, E. Bava, C. Novero: J. Appl. Phys. **63**, 1279 (1988)
12. C. Novero, H.O. Di Rocco, E. Bava, A. Godone: In preparation